City Research Online

City, University of London Institutional Repository

Article

Identification of Vibration Modes in Floating Offshore Wind Turbines

Mikel Serrano-Antoñanazas [1], Jesús-Enrique Sierra-Garcia [2,*], Matilde Santos [3] and María Tomas-Rodríguez [4]

1 Computer Science Faculty, Complutense University of Madrid, 28040 Madrid, Spain; mikeserr@ucm.es
2 Department of Digitalization, University of Burgos, 09001 Burgos, Spain
3 Institute of Knowledge Technology, University Complutense of Madrid, 28040 Madrid, Spain
4 Department of Mathematics and Engineering, City, University of London, London EC1V 0HB, UK
* Correspondence: jesierra@ubu.es

Abstract: Compared to onshore turbines, floating offshore wind turbines (FOWTs) take advantage of the increased availability of offshore wind while causing less environmental impact. However, the strong winds, waves, and currents to which they are subjected trigger oscillations that can cause significant damage to the entire structural system and reduce its useful life. To reduce these loads, active tower damping techniques such as filter banks can be used. These filters must be carefully tuned to block specific vibration frequencies. Therefore, it is essential to analyze the nature of the oscillations in the FOWT and to understand how the frequencies vary in time. This topic is usually approached from a point of view very focused on a specific turbine. What is proposed here is a general method, which can be applied to any type of wind turbine, to automatically study the relationship between vibration frequencies and the degrees of freedom (DOF) of the turbine, which facilitates the design of structural control. Each frequency is associated with the DOF of the FOWT that produces it. This methodology has been successfully validated in simulation experiments with the NREL 5 MW ITI Barge FOWT. Under the wind conditions of the experiments, the main frequency found is 0.605 Hz. This frequency coincides with the 3P theoretical frequency of the FOWT. This proposal may help to design structural control systems able to damp these vibration frequencies with accuracy and efficiency.

Keywords: wind energy; floating wind turbine; pitch control; active tower damping; vibration mode; frequency

1. Introduction

The world is now seeing a dramatic increase in energy consumption, which has led researchers to search for new sources of clean energy that leave no carbon footprint [1–3]. Wind power stands out among them as a viable and effective substitute. Wind turbines (WT) can have marine foundations or be on land. Compared to onshore turbines, offshore turbines provide several benefits, including less space restriction, more wind available offshore, and less environmental impact. Offshore wind farms have moved into the deep oceans in the last decade, with floating platforms being a viable, practical, and affordable alternative for many countries [4].

However, as these new and larger-sized floating offshore wind turbines (FOWT) are installed in deeper water, the strong winds, waves, and currents that they are subjected to may cause significant damage to the entire structural system and reduce their useful life [5]. It is therefore essential to develop control strategies to reduce these potentially damaging oscillations. The effect of the wind in the mechanical structures is not only interesting in the wind energy field, but also has been studied in civil engineering and transport [6,7].

With this aim, different passive, semiactive, and active tower damping techniques have been developed [8]. The passive methods consist of tuned mass damper (TMD) devices installed typically in the nacelle. These devices are composed of springs, dampers,

and masses that move longitudinally and/or laterally, exert forces on the nacelle, and thus reduce structural vibrations. These devices must be correctly adjusted or tuned to find the optimal parameters in such a way that the tower oscillations are damped. The semiactive methods can be seen as an evolution of the TMDs, where the coefficients of the devices (springs and dampers) are usually adjusted by closed-loop control algorithms in response to the dynamics of the structure. These methods are more flexible than passive ones and normally provide better results [9].

Finally, the active tower damping methods (ATD) are more complex and require an actuating force. In this way, an actuator inside the nacelle can be used to displace the TMD, creating an acting force that eventually could contribute towards tower oscillations' reduction. In addition to this, the pitch actuator at the rotor, which is also used to adjust the blade's angle to sustain the energy at its maximum value, can be used to lower vibration levels and reduce the acceleration at the tower top. The blades' pitch angle decreases as the tower leans upwind, increasing the amount of wind capture, increasing drag forces, and decreasing tower oscillation. In contrast, the pitch is increased when the tower leans downwind, capturing less wind, reducing drag, and decreasing the tower speed.

ATD methods require the development of control techniques in order to regulate the actuator's action. If the ATD action is not adequately designed, it could be counterproductive, causing instabilities that might damage the structure. One of the techniques recently used for this ATD design is the implementation of filter banks. These filters must be specifically tuned to block the vibration frequencies by damping the oscillations at these particular frequencies. To identify these vibration frequencies, it is essential to analyze the oscillations of the FOWT and analyze the variation in frequency with time [10]. With this aim, the well-known Fast Fourier Transform (FFT) can be used to analyze the power spectrum density (PSD) of the time window [11].

In order to address this problem, the authors propose a methodology to identify the main vibration modes in a FOWT. The floating platform of the FOWT has six main degrees of freedom (DOF), namely surge, sway, heave, roll, pitch, and yaw [12]. The proposed methodology can pair the main vibration frequency with each DOF of the turbine and analyze the influence of each DOF. This information could help to design more effective ATDs for FOWT, resulting in less turbine structural fatigue and therefore a longer useful life and lower maintenance cost. The methodology leverages the benefits of using simulation tools to study physical systems and phenomena. The simulated system may be subjected to working conditions that could degrade or even damage the real system. Furthermore, the experimental conditions can be easily adjusted as desired so that the system operates in different operating profiles, even with external and extreme events and disturbances.

In brief, the main objectives of the work can be summarized as follows:

- To develop a general methodology to find the main vibration frequencies associated with each DOF in a WT;
- To validate the approach with the NREL 5 MW ITI Barge FOWT [13];
- To identify the main vibration frequencies in the tower top acceleration of the NREL 5 MW ITI Barge FOWT.

The main benefits of this work are, on the one hand, that a methodology is proposed that allows us to systematically identify the relationship between each degree of freedom and the associated vibration frequency of a wind turbine. This knowledge is key to design controllers able to damp these vibration frequencies with accuracy and efficiency. On the other hand, it covers a gap found in the literature as this approach that studies how vibration modes in wind turbines are related to DOFs is novel. Finally, as already mentioned, this is a general methodology that can be applied to any type of wind turbine or even to real data if available.

The article has the following structure: Section 2 describes related previous works; Section 3 explains the proposed methodology used to identify the main vibration modes of the FOWT; Section 4 presents the case of use to test the methodology. Results are shown and discussed in Section 5. Finally, conclusions and future work end the paper.

2. Related Works

Since offshore structures have time-variant dynamics, it is often necessary to understand this variation in the main frequencies with time to operate with them. Time–frequency analysis methods that can describe the frequency energy intensity of a signal at various times can be used [10]. The well-known Fast Fourier Transform (FFT) is used to analyze the power spectrum of the time window, among other signal processing techniques. The importance of this analysis for the design of vibration damping systems is supported by a series of scientific publications, of which we highlight the following.

In Pezeshki et al. (2023), natural frequencies and the corresponding modes are obtained for an offshore wind turbine under the influence of wave loads [14]. An interesting finding of this work is the interpretation of the effect of the sea level variation in changing the natural frequencies. The natural periods of the floating DTU 10 MW turbine (spar, semisubmersible, and TLP FOWT) are also studied in [15], where it is shown that the motion response of the structure is dependent on the frequency of the excitation loads, as well as the wave direction.

Karimirad and Moan present a simplified method for the dynamic analysis of floating wind turbines based on the rigid body formulation [16]. It allows one to analyze the general motions and structural responses of FOWT with an acceptable degree of accuracy. In the work by Liu et al., a new time–frequency analysis method based on single mode function (SMF) decomposition is presented [10]. This method can detect three different frequencies in a simulated time-invariant signal. Using real data from vortex-induced vibration experiments, they validate the proposed SMF decomposition for vibration mode identification. Finally, field data acquired from an offshore wind turbine foundation and offshore wind turbine are analyzed. The modal identification results obtained demonstrate the efficiency of the proposed method in identifying the vibration modes.

In the case of a spar–buoy floating wind turbine, there are two main modes, the platform pitch and tower first fore–aft bending mode, according to [17]. In this paper, the authors check how modes are modified by enabling and disabling different degrees of freedom (DOF). In [18], load evaluation is conducted according to time series and FFT results. The main findings of this study relate to the problem here addressed: first, in the correlation analysis, the tower-top deflection has the highest correlation, and this further affects nacelle acceleration. Second, the tower-base pitch moment increases with the significant wave height. In ref. [19], the effect of loads (wave, wind, and dynamic bending moment) on the first natural frequency is investigated using different analysis techniques (both in the frequency and time domains) for a monopile offshore wind turbine in the North Sea. A clear correlation between load levels and the first natural frequency is demonstrated.

Niu et al. study the influence of scour in the layered foundations on the first natural frequency of a monopile wind turbine [20]. By performing model experiments on a typical built three-layered foundation prototype and with a theoretical analysis, the variations in the first natural frequency of the monopile at different scour depths are obtained. The FFT is used to analyze the acceleration signals of each experimental condition.

A recent study by Zeng obtains the higher-harmonic wave loads and low-frequency resonance response of the DeepCWind semi-submersible floating offshore wind turbine by the phase decomposition method [21]. They use a high-fidelity CFD solver to investigate the interaction process of extreme waves and the low-frequency resonant response.

Deng et al. investigate how the frequency-dependent characteristics of aerodynamic damping influence the dynamic responses of a floating offshore wind turbine [22]. They use an aero-hydro-servo-structure coupled model for the OC4 DeepCWind wind turbine and confirm the close relationship between aerodynamic damping and the natural periods of platform motion.

From another perspective, the work presented in [23] identifies modal parameters by using converted displacements from measured accelerations and applies this strategy to monopile offshore wind turbines.

As seen, some previous works have studied the frequency spectrum of the oscillation signals in wind turbines. However, in the related literature, there are few works that study the relationship between DOFs and vibration modes in wind turbines. In fact, to our knowledge, there is, until now, no method to automatically obtain the turbine vibration frequencies associated with each degree of freedom. To cover this gap, a methodology is proposed that allows the main vibration frequencies to be identified and can be used with any type of wind turbine. Although this methodology is validated with the FOWT NREL 5 MW ITI Barge, it is general and it can be applied to any type of offshore turbine, both bottom-fixed and floating—an aspect that the articles shown in the state of the art lack since they are specific to a certain type of turbine.

3. Methodology for Identification of Vibration Modes of a Wind Turbine

The methodology here proposed identifies the vibration modes of FOWT. It is mainly based on the deactivation of the various DOFs and subsequent use of the PSD function. The output of this methodology provides the main frequency peak for each DOF of the FOWT.

Figure 1 shows the general identification procedure for a signal X_t of the FOWT. This process can be applied to any signal obtained by the high-fidelity wind turbine simulator OpenFast or to signals obtained by any simulation tool able to configure wind turbine DOFs.
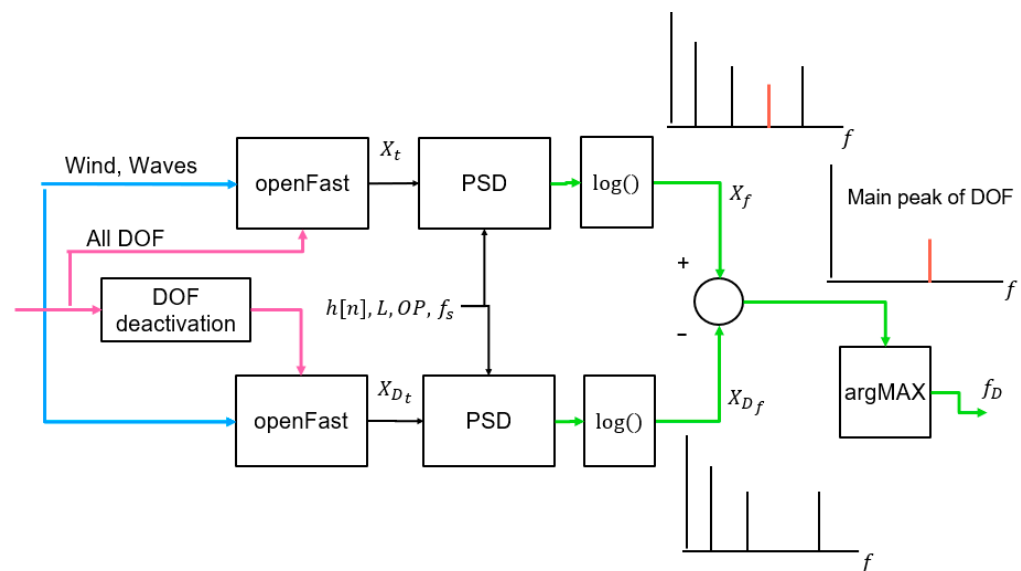

Figure 1. Methodology for the identification of vibration modes in FOWT.

First, a simulation with all the DOFs activated is carried out and wind and wave conditions are set up. The signal X_t in the time domain is extracted from the simulation. This signal X_t can be any mechanical signal obtained with the simulation tool, such as the top tower displacement, the platform pitch, the yaw bearing acceleration, etc. Then, the PSD is applied to obtain the coefficients of the power spectral density, X_f. There are different methods to estimate the PSD, such as Barlett's method or Welsch's method. We use the latter. To run Welsch's method, it is necessary to select a windowing function $h(n)$. The Hamming window is chosen as it provides a good frequency resolution. At the output of the PSD block, the coefficients of the PSD feed a logarithmic block to facilitate the comparison.

After this step, a new simulation with the same wind and wave conditions is carried out. The difference from the previous execution is that, in this case, the DOF whose influence is to be studied is deactivated. Then, the same signal is extracted from the simulation environment, denoted X_{Dt}, because a DOF has been deactivated. Again, the PSD is applied to obtain the power spectral density. These coefficients are stored in X_{Df}.

These sequences are subtracted to determine the presence of peaks that are present in X_f but not in X_{Df}.

The signals X_t and X_{D_t} can be real-life or simulated signals. However, we focus on the simulated ones because, in a real wind turbine, all DOFs are active and none of them can be deactivated. For example, it is not easy to lock the pitch motion of the platform to study what happens when this DOF is not active. Furthermore, replicating the same experimental conditions with and without DOFs would be infeasible with a real turbine since the experimental environment is subject to random events such as wind and waves.

To formalize the methodology, first, the logarithmic PSD is obtained; see (1) and (2).

$$X_f(k) = 10 \, log_{10} \left(\frac{1}{KLU} \sum_{i=0}^{K-1} \left| \sum_{n=0}^{L-1} h(n) X_t((n+i \cdot OP)T_s)e^{-\frac{2\pi jkn}{L}} \right|^2 \right) \tag{1}$$

$$X_{D_f}(k) = 10 \, log_{10} \left(\frac{1}{KLU} \sum_{i=0}^{K-1} \left| \sum_{n=0}^{L-1} h(n) X_{D_t}((n+i \cdot OP)T_s)e^{-\frac{2\pi jkn}{L}} \right|^2 \right) \tag{2}$$

where $j = \sqrt{-1}$, $h(n)$ is the sequence of coefficients of the windowing function, T_s is the sampling time, OP is the overlapping, L is the window size, K is the number of windows in the time sequence, and U is a coefficient that varies with the windowing function according to Equation (3). D denotes the DOF that is studied, f_D is the frequency of the main peak associated with the DOF D in Hz, and X_t is the signal used to analyze the vibration.

$$U = \frac{1}{L} \sum_{n=0}^{N-1} |h(n)|^2 \tag{3}$$

In this case, the Hamming window given by Equation (3) is used.

$$h(n) = a_0 - a_1 \cos\left(\frac{2\pi n}{N-1}\right), \quad a_0 = 0.5383, \; a_1 = 0.4616 \tag{4}$$

Once the logarithmic PSDs are obtained, they are compared to obtain the location of the main peak (5).

$$f_D = \underset{i \in \{\mathbb{N} \cup 0\} < L}{\mathrm{argMAX}} \left(X_f(i) - X_{D_f}(i) \right) \frac{1}{T_s \cdot L} \tag{5}$$

The values of L, T_{sim}, and T_s must be carefully selected to comply with the following constraints. First, the Nyquist criteria must be fulfilled; therefore, the sampling frequency must be larger than double the maximum frequency of the signal with the largest frequency, f_{max}.

$$f_s > 2f_{MAX} \rightarrow T_s < \frac{1}{2f_{MAX}} \tag{6}$$

To guarantee specific accuracy in the study of the frequency spectrum, called Δf, the number of samples in the window, L, must be set accordingly (7).

$$L \geq \frac{1}{T_s \cdot \Delta f} \tag{7}$$

The relationship between the total number of samples N and L, K, and OP is given by (7):

$$N = L + OP(K-1) \tag{8}$$

Then, considering that the total simulation time is $T_{sim} = N \cdot T_s$, to guarantee a determined number of windows K, the T_{sim} must be sufficiently long. That is,

$$T_{sim} \geq T_s(L + OP(K-1)) + T_w \tag{9}$$

where T_w denotes the warm-up period, which is the initial transitory phase of the simulation that must be discarded.

In Figure 1, the PSD is used instead of directly the FFT because, as is well known, the FFT of length N of a signal sampled with a sampling frequency f_s provides N samples of the Fourier transform of a signal between frequencies 0 and f_s. The frequency interval between two consecutive samples in the frequency domain is $f_s/(N-1)$.

In other words, the results of an FFT are strongly related to the number of signal samples available in the time domain. If this number of samples is less than N, zero values are added to the end of the signal to reach the necessary N values. If the number of samples is greater than N, only the first N values are used to calculate the FFT, and the last few values of the signal are discarded. Thus, this technique is limited to a certain window of samples.

However, the PSD applies a sliding window in the time domain to the signal under consideration. For each window, the FFT is calculated. The results are obtained as the mean of the square of the modulus of all these FFTs. Therefore, the PSD is a more accurate estimate of the frequency spectrum than the FFT and can be applied to signal sequences of any length.

As a simulation tool, the use of OpenFast is proposed. OpenFAST is a multi-physics, multi-fidelity tool to simulate the coupled dynamic responses of wind turbines. OpenFAST couples computational modules for aerodynamics, hydrodynamics for offshore structures, control and electrical system (servo) dynamics, and structural dynamics to enable coupled non-linear aero-hydro-servo-elastic simulation in the time domain. The main code and underlying modules are mostly written in Fortran, and modules can also be written in C [24].

Table 1 summarizes the main variables provided by OpenFast [23] to study the vibrations in the WT; other simulation tools give similar information.

Table 1. Possible signals provided by OpenFast to study the vibrations.

Variables	Description
NcIMU (T/R) (V/A) ($x/y/z$) s	Nacelle inertial measurement unit (Translational/Rotational) (Velocity/Acceleration) along ($x/y/z$) axis
YawBrTD ($x/y/z$) (p/t)	Tower-top/yaw bearing fore–aft translational deflection along ($x/y/z$) (p-axis/t-axis)
YawBrTA ($x/y/z$) p	Tower-top/yaw bearing fore–aft translational acceleration along ($x/y/z$) p-axis
YawBrRD ($x/y/z$) t	Tower-top/yaw bearing fore–aft rotational deflection along ($x/y/z$) t-axis
YawBrR (V/A) ($x/y/z$) p	Tower-top/yaw bearing fore–aft rotational (Velocity/Acceleration) along ($x/y/z$) p-axis
PtfmT (D/V/A) ($x/y/z$) (t/i)	Platform (x: surge/y: sway/z: heave) translational (Displacement/Velocity/Acceleration) along ($x/y/z$) (t/i) axis
PtfmRD ($x/y/z$) i	Platform (x: surge/y: sway/z: heave) rotational displacement along ($x/y/z$) i-axis
PtfmR (V/A) ($x/y/z$) (t/i)	Platform (x: surge/y: sway/z: heave) rotational (Velocity/Acceleration) along ($x/y/z$) (t/i) axis

As explained in [25], the DOF determines the physical phenomena simulated, the degree of variability of the signals, and thus the fidelity of the simulation. Normally, considering more DOFs gives more reliable results, but, in contrast, it also increases the computational cost. In a wind turbine, the main physical phenomena that can be included or neglected in the simulation are the bending of the various system elements, the deformation of the blades, and the translation and rotation of the platform. A complete list of DOFs that can be configured in OpenFast is shown in Table 2 and illustrated in Figure 2.

Table 2. OpenFast degrees of freedom.

| Variable	Description
FlapDOF1	First flapwise blade mode
FlapDOF2	Second flapwise blade mode
EdgeDOF	First edgewise blade mode
DrTrDOF	Drivetrain rotational flexibility
GenDOF	Generator
YawDOF	Yaw
TwFADOF1	First fore–aft tower bending mode
TwFADOF2	Second fore–aft tower bending mode
TwSSDOF1	First side-to-side tower bending mode
TwSSDOF2	Second side-to-side tower bending mode
PtfmSgDOF	Platform horizontal surge translation
PtfmSwDOF	Platform horizontal sway translation
PtfmHvDOF	Platform vertical heave translation
PtfmRDOF	Platform roll tilt rotation
PtfmPDOF	Platform pitch tilt rotation
PtfmYDOF	Platform yaw rotation
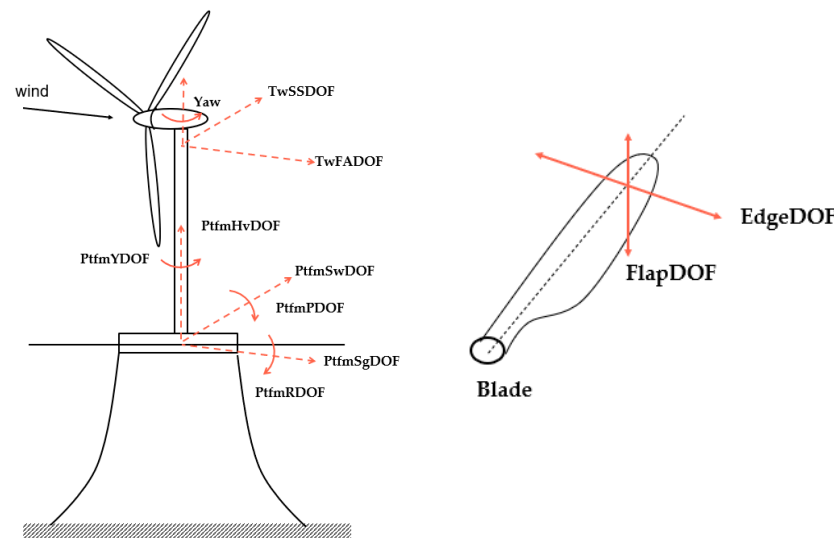
Figure 2. Degrees of freedom in an offshore wind turbine modeled by OpenFast.

One of the limitations of the proposed method is that its application is limited to the DOFs that the software simulation tool can model, although, in general, tools such as OpenFAST consider most of them. For example, there are works that include up to 16 DOFs [26]. Another aspect that could be considered a limitation is that the results refer to specific wind and wave conditions. However, the process can be repeated with different conditions. Finally, as the results are obtained numerically using a software simulation tool, the computational limitations of the simulation tool and the computer must be considered, both in precision and computational time.

4. Use Case: 5 MW ITI Barge Wind Turbine

At present, mainly four types of FOWT can be distinguished (Figure 3), corresponding to possible solutions to the stability problem [8].
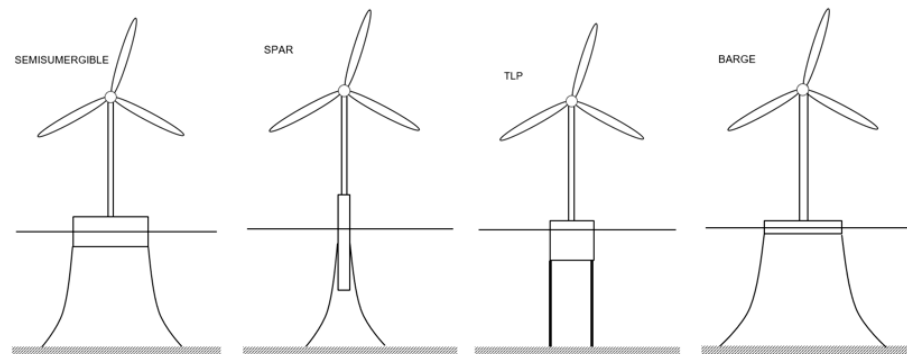
Figure 3. Types of floating offshore wind turbines.

- Semi-submersible structures: part of the structure is submerged, and the other part protrudes from the sea surface, with mooring lines to the ground.
- Spar structure (buoy): it consists of a cylindrical structure almost entirely submerged, with a counterweight at the end to give stability to the wind turbine (center of gravity of the platform as low as possible, below the center of buoyancy) so that it can withstand the loads produced by wind and waves. It has the lowest structural cost. It is also anchored to the ground by cables.
- Tension leg platform (TLP) structure: the mooring cables are tensioned, allowing some horizontal movement but providing vertical stability against waves and wind. It is the most firmly attached to the seabed. The critical part of the design lies precisely in the difficulty of its installation due to the anchoring of the cables to the sea bottom and to the fact that, as a consequence of the tension to which they are subjected, not all types of seabed are suitable for such mooring.
- Flotation-stabilized structure (barge): this is a light structure with a large surface area (pontoon), which gives the whole structure a certain stability due to the inertia of the added mass. It is also anchored to the bottom by means of cables to prevent the wind turbine from overturning or drifting.

To validate this methodology, we use the NREL 5 MW ITI Barge Wind Turbine under its nominal operation conditions. This FOWT belongs to the last category of the list above (barge type). The main parameters of this wind turbine are listed in Table 3. This specific wind turbine is chosen due to the large number of DOFs that can be studied in OpenFast. This is a widely studied FOWT in the scientific literature, being used as a benchmark in several contributions.

Table 3. Main parameters of the NREL 5 MW ITI Barge Wind Turbine [10].

Parameter	Value
Rated wind speed	11.4 m/s
Cut-out wind speed	25 m/s
Nominal rotor speed	12.1 rpm
Blade length	61.609 m
Hub height	90 m
Rated generator torque	43,093 Nm
Maximum generator torque	47,402 Nm
Power rating	5 MW

In this work, two signals are studied: the tower-top/yaw bearing fore–aft translational acceleration along the xp-axis (YawBrTAxp) and the tower-top/yaw bearing side-to-side (translational) acceleration along the yp-axis (YawBrTAyp). These signals are defined in the FAST user's manual [24]. The yaw bearing point is located at the center of the bearing between the tower and the nacelle. This bearing is needed to support the rotation of the nacelle around the yaw axis. In Figure 4, the location of the yaw bearing point is shown.
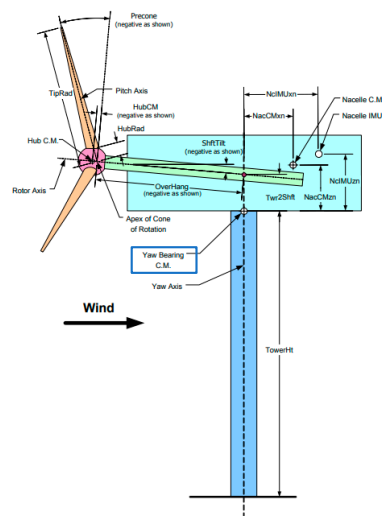
Figure 4. Location of the yaw bearing point [24].

To better visualize the signals YawBrTAxp and YawBrTAyp, and the DOFs of Table 2, the coordinate system defined in the manual of HydroDyn is shown in Figure 5. The *x*-axis is aligned with the fore–aft direction. The *z*-axis is aligned with the yaw axis. Finally, the *y*-axis is perpendicular to the *x*–*z* plane.
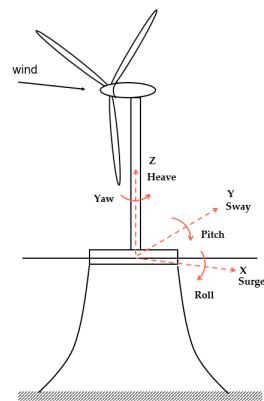

Figure 5. FWOT coordinate system.

In principle, the proposed methodology could be applied to various wind and wave conditions. However, to clearly identify the frequencies for each DOF, it is recommended not to include turbulence or wave disturbances. Thus, in this work, the environmental conditions used to identify the main frequencies are as follows.

- Wind speed: 13 m/s. It ensures that the turbine is operating at the rated power and generator speed.
- Wind turbulence: Steady, no turbulence. In this way, the frequencies are shown without wind disturbances.
- Wave mode: None, still water. It allows us to study the frequency spectrum without being affected by wave disturbances.

    Regarding the parameters N, T_s, and T_{sim}, these are set as follows.

- T_s = 12.5 ms. This is the recommended value in OpenFast. Following the Nyquist theorem, signals with frequencies below 40 Hz can be sampled without losing information. Frequencies larger than 40 Hz are not relevant in FOWT.
- L: 27307. With this window size and the chosen T_s, the frequency resolution is 2.93 mHz. This resolution is sufficient to accurately identify the main vibration modes.
- OP = 0.9 L. This means that 90% of window overlapping is considered.

- $K = 9$. This number of windows ensures that enough time is provided to study the signal and draw conclusions about the frequencies.
- $T_{sim} = 3000$ s. This time is large enough to ensure the sampling K windows of size L with an overlapping OP.
- $T_w = 1500$ s. The warm-up period depends on the turbine's technical characteristics. In order to set a suitable value, it is recommended to perform a visual inspection of the output signal when all DOFs are active. According to the simulation results, we set 1500 s as a conservative value (see Figure 5), although this value could be reduced.

The simulation time of the experiments is 4500 s. However, the first 1500 s are discarded as a warm-up initial period (transient part of the signal) due to the fact that the platform oscillation and rotation signals need some time to reach the steady state. Figures 5 and 6 show the main displacement and rotational responses of the FOWT. It is possible to observe the transitory behavior during the initialization.
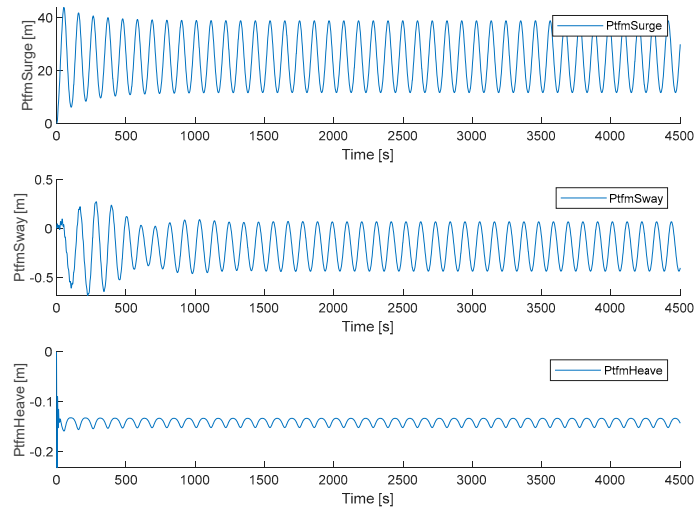

Figure 6. ITI Barge Floating Wind Turbine, floating platform displacement signals.

In the real system, the signal YawBrTAxp can be measured with an accelerometer, and the signals shown in Figures 6 and 7 are obtained by integrating the information provided by an accelerometer located in the platform. In the simulation, these signals are calculated using the aero-hydro-servo-elastic model embedded in OpenFAST [24].
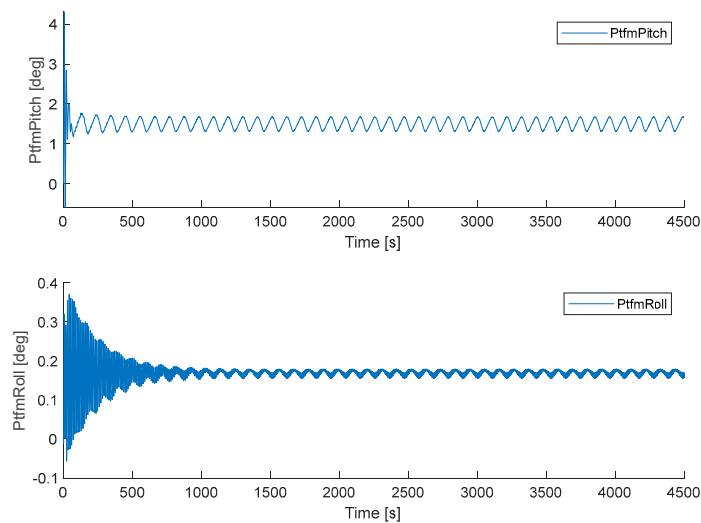

Figure 7. ITI Barge Floating Wind Turbine, floating platform rotation signals.

5. Simulation Results and Discussion

As mentioned previously, the software OpenFast 3.5.0 [23] developed by NREL was used to simulate a nonlinear floating wind turbine. The PSD and the data processing were implemented in Matlab/Simulink.

Simulink is a block diagram environment used to design systems with multi-domain models, simulate them before implementing them in hardware, and deploy them without writing code [27]. MATLAB is a programming and numerical computing platform used by millions of engineers and scientists to analyze data, develop algorithms, and create models. MATLAB combines a refined desktop environment for iterative analysis and design processes with a programming language that expresses the mathematics of matrices and arrays directly [28].

In Sections 5.1–5.13, the influence of each DOF is independently studied (Figures 8–20). In the last subsection, all vibration modes are presented together, and the main vibration frequencies are summarized (Figure 21 and Table 4).

5.1. Influence of First Fore–Aft Tower Bending (TwFADOF1) and the 3P

Figure 8 compares the power spectrum density of the YawBtTAxp and YawBtTAyp, when TwFADOF1 is activated (blue line) and deactivated (red line). The most damped peak is at 0.605 Hz. The peaks with frequencies larger than this seem to be slightly damped.
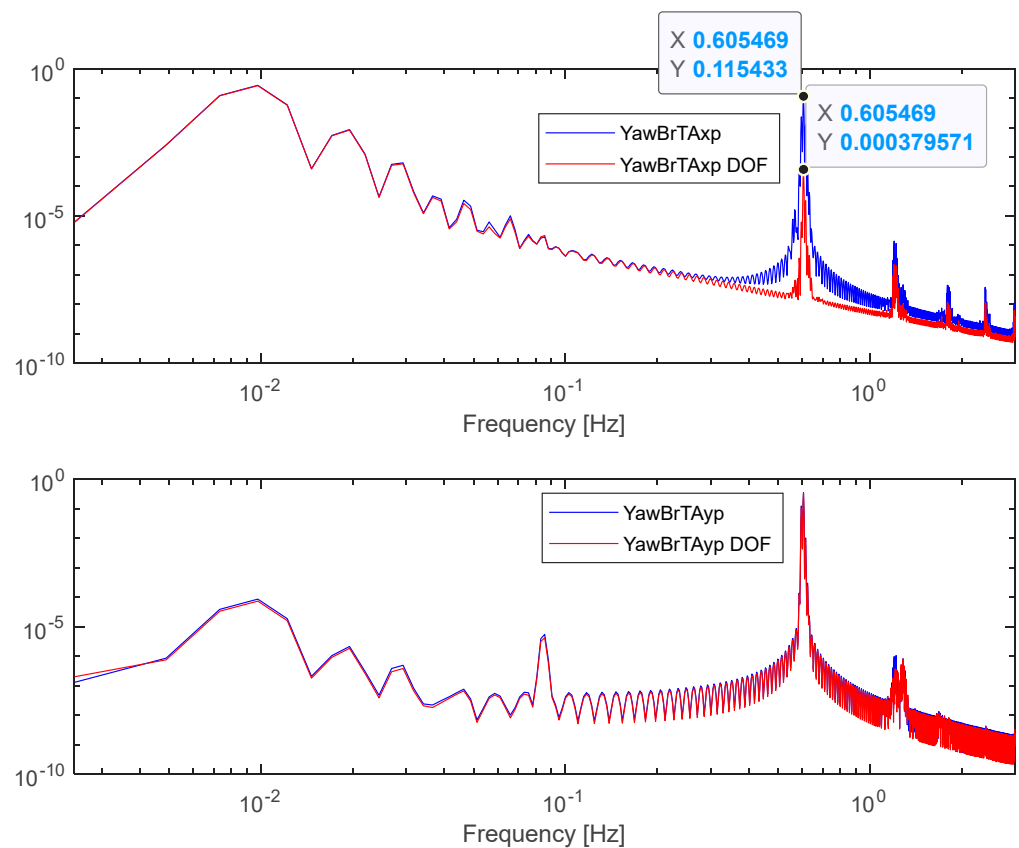

Figure 8. Tower top acceleration, PSD with TwFADOF1 deactivated.

However, low-frequency modes are not affected. The side-to-side signal is not apparently influenced. Only a very small variation is observed in one of the small peaks.

Another interesting point that can be drawn from these figures is that the 3P frequency is observed in the frequency spectrum. This effect is produced by the tower shadow when the blades are rotating [29]. It can be theoretically calculated using (10).

$$3P[\text{Hz}] = n_{blades} \cdot \frac{w\,[\text{rpm}]}{60\,[\text{s}/\text{min}]} = 3 \cdot \frac{12.1}{60} = 0.605\,\text{Hz} \tag{10}$$

where n_{blades} is the number of blades and w is the angular rotor speed—in this case, the rated value. At 0.605 Hz, we can observe a peak in both lines, red and blue. When the TwFADOF1 is deactivated, the peak still appears at this frequency because it is caused by the 3P frequency. When the TwFADOF1 is active, the amplitude of the peak grows due to the effect of the first fore–aft tower bending oscillation.

Other simulations were carried out at a 9 m/s wind speed with a rotor angular speed of 10 rpm, and at a 7 m/s wind speed with a rotor angular speed of 8.44 rpm. In the first case, the 3P was observed at 0.5 Hz and, in the second case, at 0.42 Hz. This corroborates Equation (10).

It is noteworthy that, at the rated speed, the frequency 3P matches the frequency associated with TwFADOF1; thus, it is key to apply ATD strategies to mitigate this effect.

5.2. Influence of Second Fore–Aft Tower Bending (TwFADOF2)

Figure 9 compares the power spectrum density of the YawBtTAxp and YawBtTAyp, when TwFADOF2 is activated (blue line) and deactivated (red line). In this case, the most damped peak is at 3 Hz, so this must be the second tower fore–aft. Lower frequencies are not affected. There is no apparent influence in side-to-side modes.
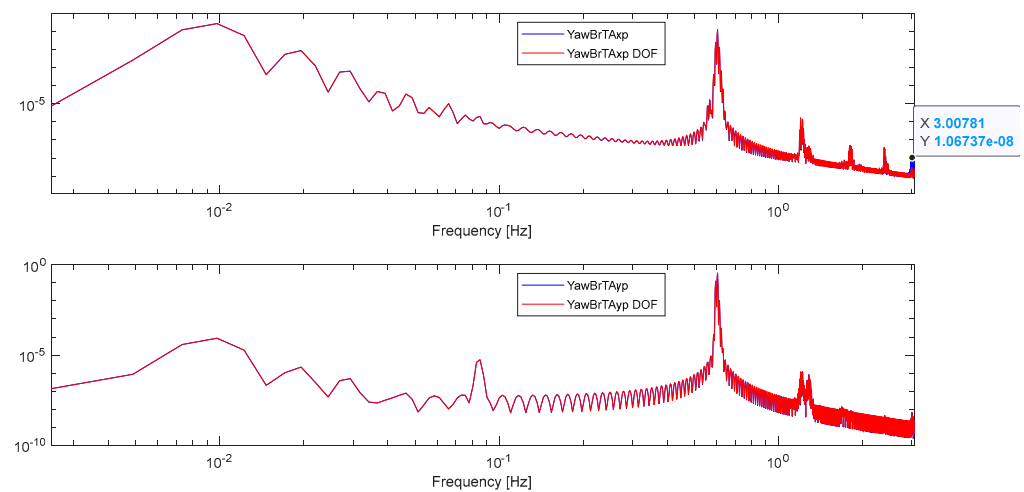

Figure 9. Tower-top acceleration, PSD with TwFADOF2 deactivated.

5.3. Influence of First Side-to-Side Tower Bending (TwSSDOF1)

Figure 10 compares the power spectrum density of the YawBtTAxp and YawBtTAyp, when TwSSDOF1 is activated (blue line) and deactivated (red line). The most damped peak in signal YawBtTAyp occurs at 0.605 Hz, which seems to be the first tower side-to-side mode. Moreover, the peaks at 0.085 Hz and 1.20 Hz are damped. The low frequencies are not affected by this DOF. As expected, this TwSSDOF1 degree of freedom does not affect the fore–aft axis.
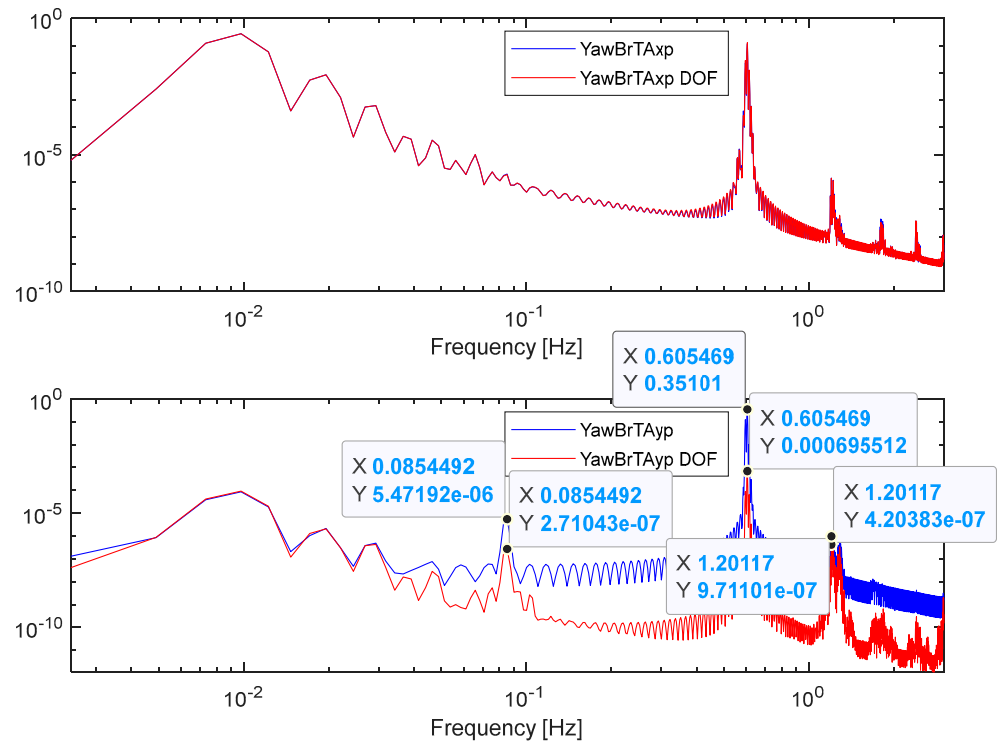
Figure 10. Tower-top acceleration, PSD with TwSSDOF1 deactivated.

5.4. Influence of Second Side-to-Side Tower Bending (TwSSDOF2)

Figure 11 compares the power spectrum density of the YawBtTAxp and YawBtTAyp, when TwSSDOF2 is activated (blue line) and deactivated (red line). The frequency component at 3 Hz on the *y*-axis is better damped now. It is also possible to see how the remaining spectra are essentially not influenced.
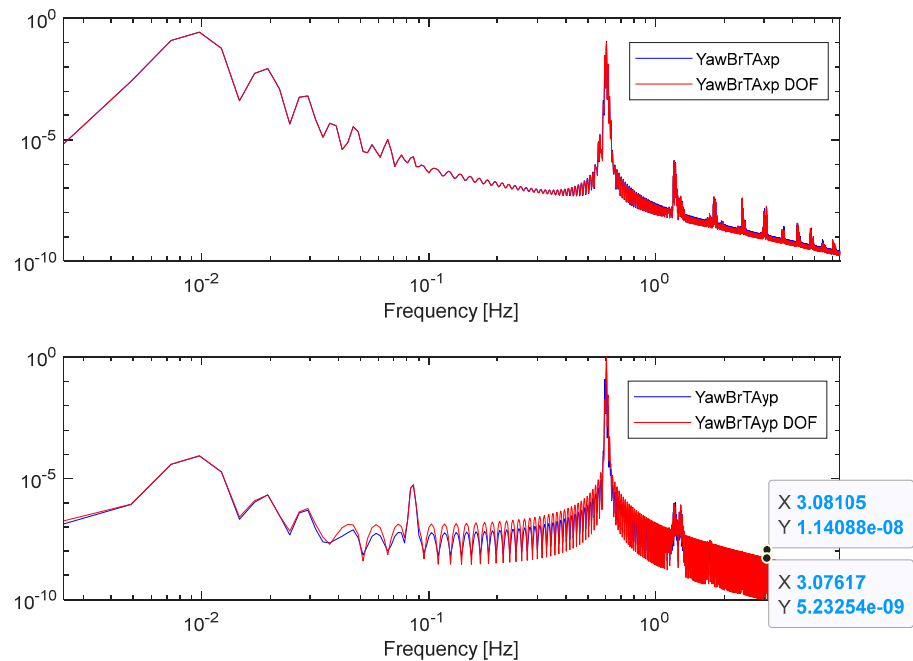
Figure 11. Tower-top acceleration, PSD with TwSSDOF2 deactivated.

5.5. Influence of First Flapwise (FlapDOF1)

Figure 12 compares the power spectrum density of the YawBtTAxp and YawBtTAyp, when FlapDOF1 is activated (blue line) and deactivated (red line). This DOF mainly affects the side–side oscillations, especially at 0.0097 Hz, which shows an increase in gain at low frequencies, but it is damped from 0.085 Hz onwards. In the fore–aft direction, acceleration seems to be damped from 0.6 Hz onwards.
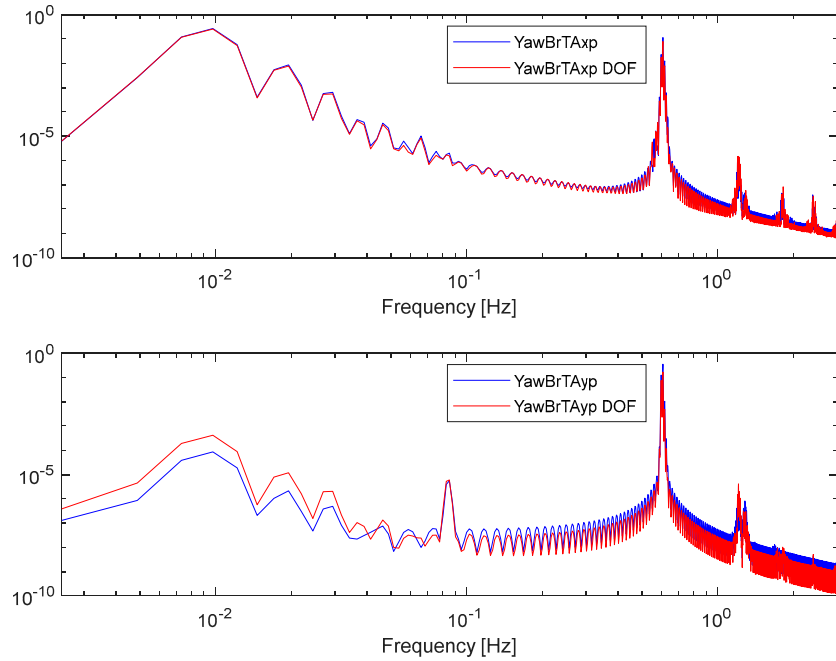

Figure 12. Tower-top acceleration, PSD with FlapDOF1 deactivated.

5.6. Influence of Second Flapwise (FlapDOF2)

Figure 13 compares the power spectrum density of the YawBtTAxp and YawBtTAyp, when FlapDOF2 is activated (blue line) and deactivated (red line). Although the DOF related to the first mode of the flap affects the signals, the second mode (FlapDOF2) does not seem to affect them. Only slight damping at 3 Hz in the fore–aft oscillation is observed.
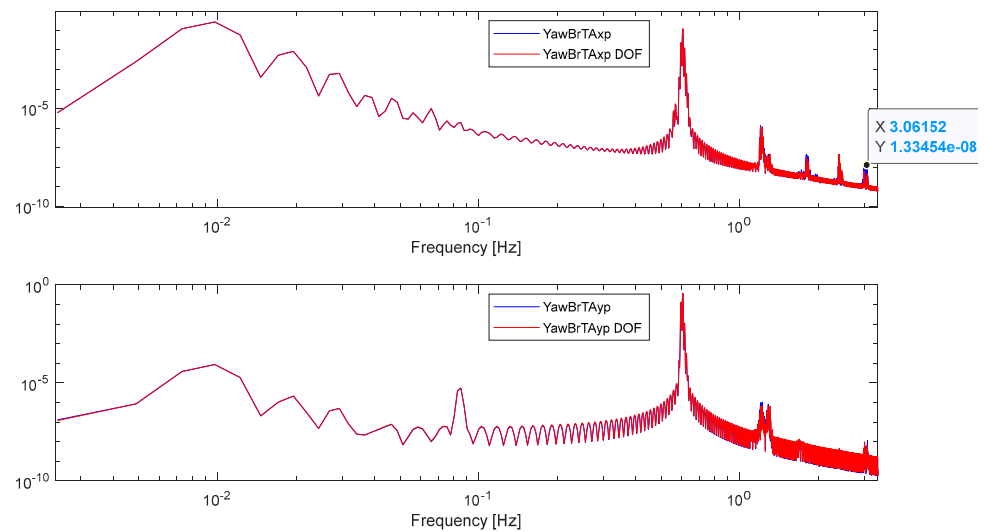

Figure 13. Tower-top acceleration, PSD with FlapDOF2 deactivated.

5.7. Influence of First Edgewise (EdgeDOF)

Figure 14 compares the power spectrum density of the YawBtTAxp and YawBtTAyp, when EdgeDOF is activated (blue line) and deactivated (red line). In this case, a subtle damping of the frequency peak at 1.28 Hz in the fore–aft and side–side oscillations is observed. In addition, a smooth variation in the medium frequencies of the YawBtTAyp can be noted but without affecting the peak at 0.85 Hz.
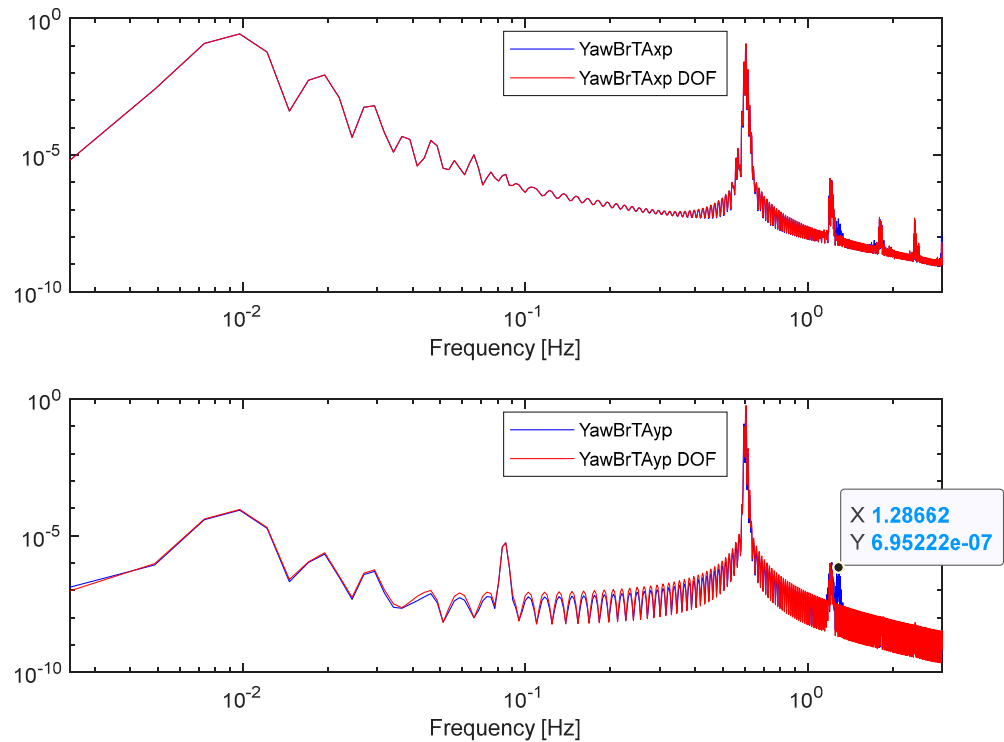

Figure 14. Tower-top acceleration, PSD with FlapDOF2 deactivated.

5.8. Influence of Platform Horizontal Surge Translation (PtfmSgDOF)

Figure 15 compares the power spectrum density of the YawBtTAxp and YawBtTAyp, when PtfmSgDOF is activated (blue line) and deactivated (red line). The main peak at 0.0097 Hz is very damped on the *x*- and *y*-axis. The peak at 0.085 Hz is also damped in the side–side acceleration plot. The peak at 0.6 Hz is not affected by this DOF, although the gain at higher frequencies seems to be more damped in the fore–aft direction. The peak in fore–aft is much more affected than in the side–side axis due to the fact that the surge is aligned with the fore–aft motion (Figure 5). As expected, the platform affects the low frequencies of the system due to its large mass.
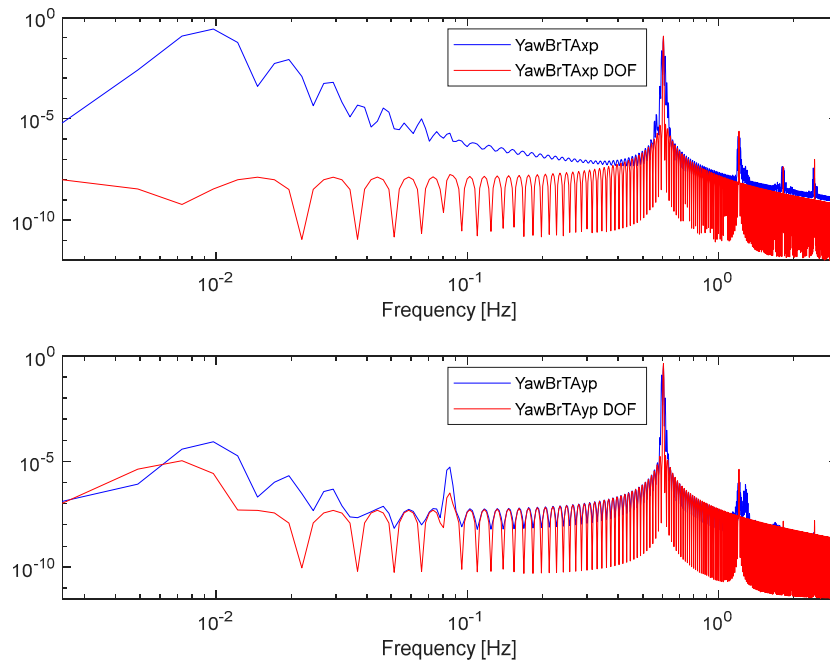
Figure 15. Tower-top acceleration, PSD with PtfmSgDOF deactivated.

5.9. Influence of Platform Horizontal Sway Translation (PtfmSwDOF)

Figure 16 compares the power spectrum density of the YawBtTAxp and YawBtTAyp, when PtfmSwDOF is activated (blue line) and deactivated (red line). The fore–aft motion is not affected. However, the side–side spectrum is damped for the entire frequency range. Moreover, the peak at 0.085 Hz is almost totally absorbed. This result is also reasonable as the sway translation of the platform is aligned with the *y*-axis (Figure 5).
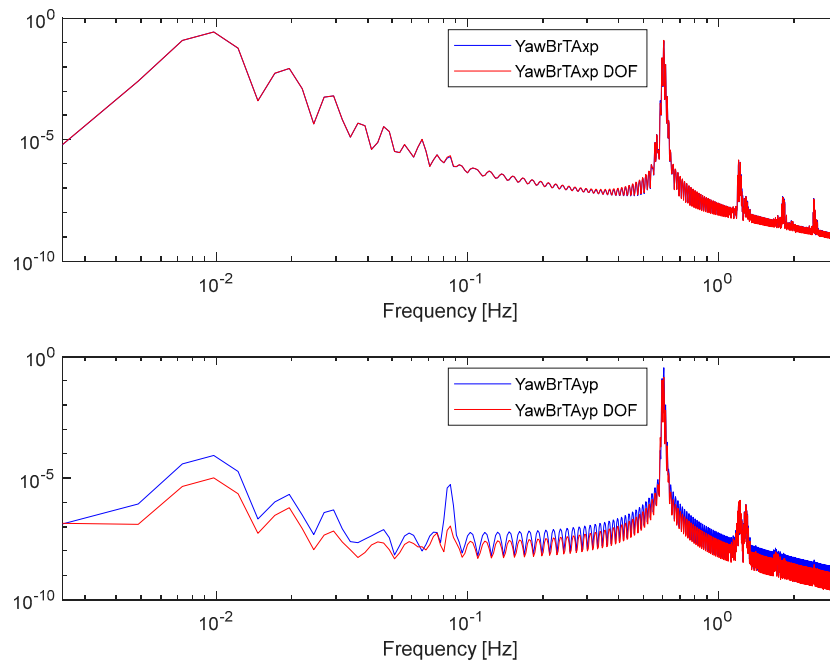

Figure 16. Tower-top acceleration, PSD with PtfmSwDOF deactivated.

5.10. Influence of Platform Vertical Heave Translation (PtfmHvDOF)

Figure 17 compares the power spectrum density of the YawBtTAxp and YawBtTAyp, when PtfmHvDOF is activated (blue line) and deactivated (red line). No frequencies in

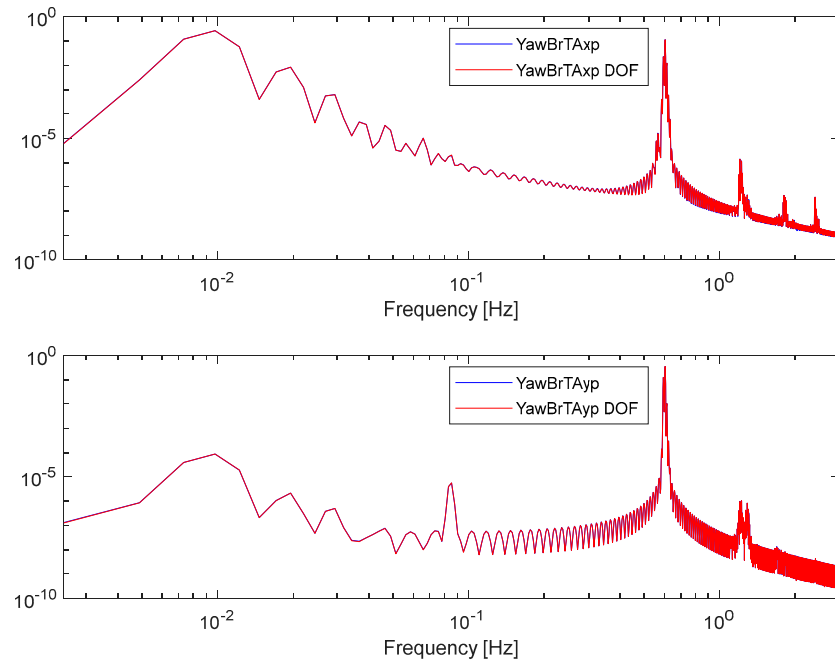the fore–aft or side–side are affected; indeed, the blue and red lines completely overlap in both figures.

Figure 17. Tower-top acceleration, PSD with PtfmHvDOF deactivated.

5.11. Influence of Platform Roll Tilt Rotation (PtfmRDOF)

Figure 18 compares the power spectrum density of the YawBtTAxp and YawBtTAyp, when PtfmRDOF is activated (blue line) and deactivated (red line). As expected, this DOF does not affect the fore–aft direction. This may be explained by the fact that the roll axle is aligned with the *x*-axis. In contrast, in the side–side direction, all frequencies are damped except the peaks appearing at 0.0097 Hz and 1.2 Hz.
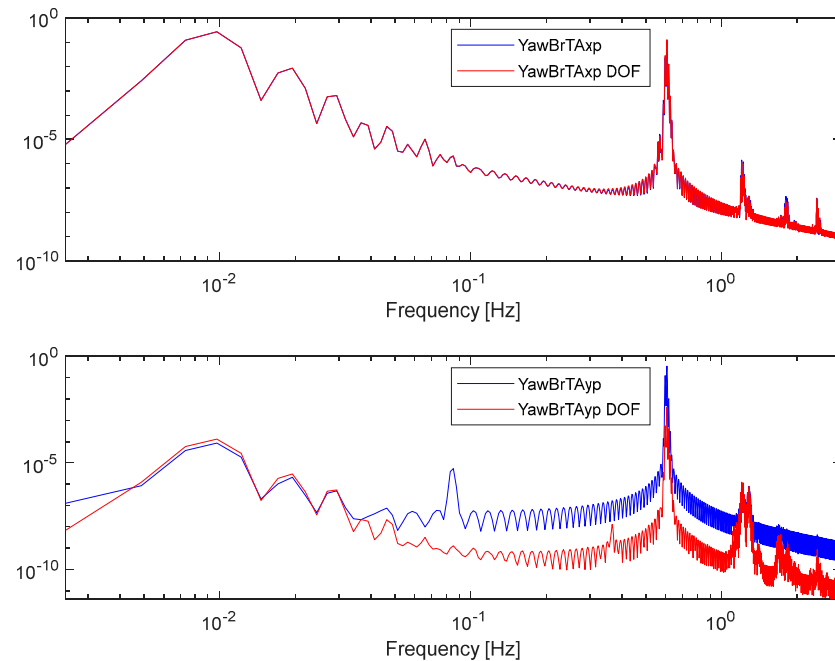

Figure 18. Tower-top acceleration, PSD with PtfmRDOF deactivated.

5.12. Influence of Platform Pitch Tilt Rotation (PtfmPDOF)

Figure 19 compares the power spectrum density of the YawBtTAxp and YawBtTAyp, when PtfmPDOF is activated (blue line) and deactivated (red line). Tower-top acceleration along the *x*-axis has the peak at 0.6 Hz damped, so this rotation seems to be coupled with the first tower fore–aft bending. However, it is interesting to note that the contribution of the first fore–aft tower bending (TwFADOF1) to the YawBtTAxp is much larger than the contribution of the platform pitch. Moreover, oscillations appearing at frequencies between 0.035 Hz and 0.09 Hz are damped too. On the other hand, there is very little damping on the side–side oscillation.
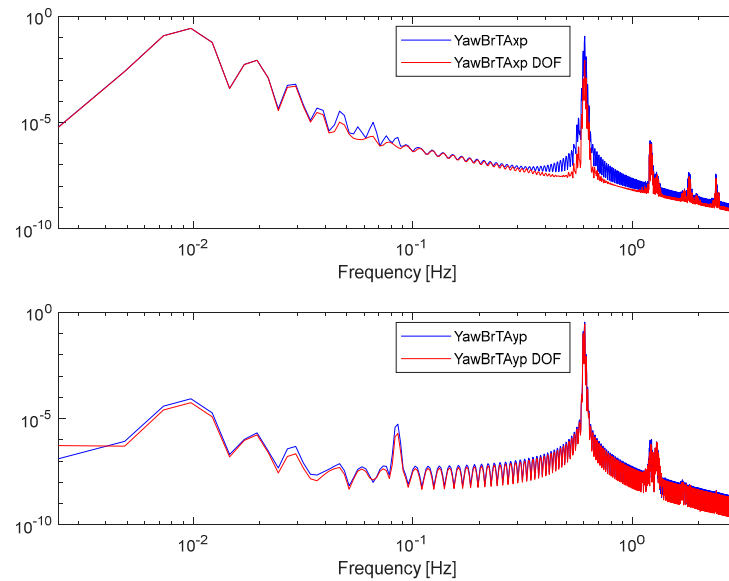

Figure 19. Tower-top acceleration, PSD with PtfmPDOF deactivated.

5.13. Influence of Platform Yaw Rotation (PtfmYDOF)

Figure 20 compares the power spectrum density of the YawBtTAxp and Yaw-BtTAyp, when PtfmYDOF is activated (blue line) and deactivated (red line). It seems that the fore–aft oscillation is not affected by this DOF and there is a very little damping in the side–side direction.
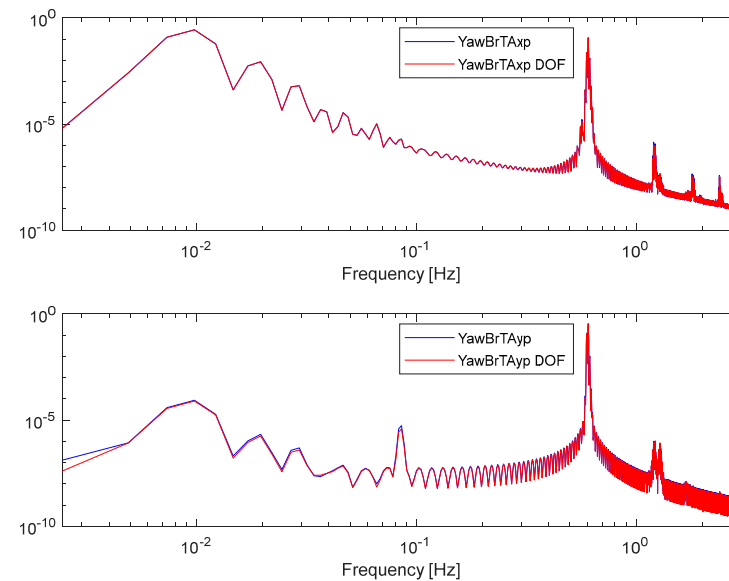

Figure 20. Tower-top acceleration, PSD with PtfmYDOF deactivated.

5.14. Discussion of the Results

Figure 21 shows the power spectrum density of the response of the turbine when all DOFs are active. In this figure, the main DOFs are shown at each respective frequency. The frequency of each DOF was obtained following the methodology described in Section 3.

It is possible to see how, in the fore–aft direction, the platform surge has the largest contribution to the power spectrum, followed by the 3P frequency. In the case of the side–side direction, the latter exhibits the largest peak. Due to the platform's large mass and inertia, the lowest vibration frequencies are derived from this element. It is also noticeable that the amplitude decreases with the frequency; indeed, the smallest peak appears at 3 Hz.
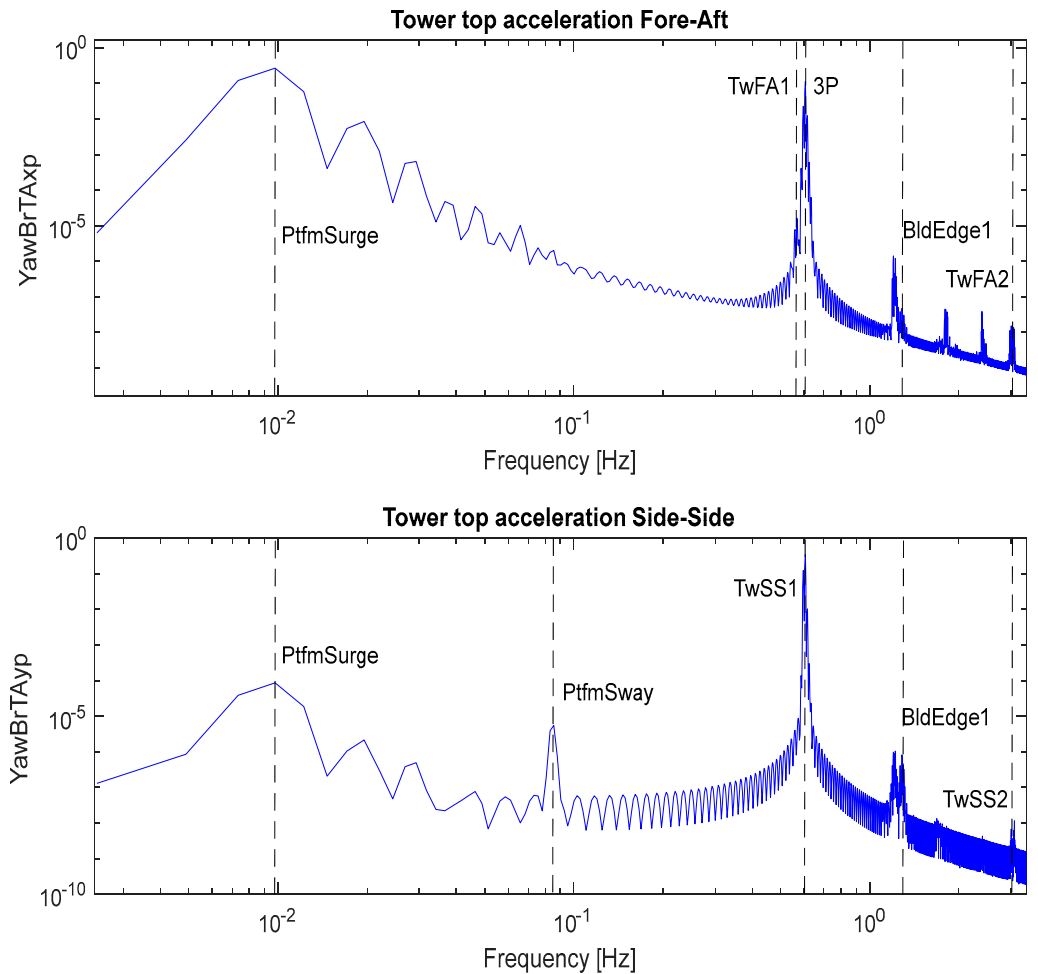

Figure 21. Tower-top acceleration, PSD with all DOFs active.

Table 4 summarizes the main vibration frequencies identified for each DOF. If no relevant change in the power spectrum is observed, it is indicated as "Not affected" in the table. The lowest frequencies arise from the platform's translational DOFs, PtfmSgDOF and PtfmSwDOF, due to the large mass of the platform. Interestingly, the DOF that corresponds to the flexibility of the blade, FlapDOF1, also introduces a low-frequency oscillation. The largest frequency, 3 Hz, is related to the second bending mode of the tower. This value appears for both the fore–aft and side–side directions.

Table 4. Identification of frequencies when each DOF is deactivated.

DOF	Frequency in YawBrTAxp Fore–Aft [Hz]	Frequency in YawBrTAyp Side–Side [Hz]
FlapDOF1	Not affected	0.0097
FlapDOF2	Not affected	Not affected
EdgeDOF	1.28	1.28
YawDOF	Not affected	Not affected
TwFADOF1	0.605	Not affected
TwFADOF2	3	Not affected
TwSSDOF1	Not affected	0.605
TwSSDOF2	Not affected	3
PtfmSgDOF	0.0097	Not affected
PtfmSwDOF	Not affected	0.085
PtfmHvDOF	Not affected	Not affected
PtfmRDOF	Not affected	0.6 and 0.085
PtfmPDOF	Not affected	Not affected
PtfmYDOF	0.6	0.085

While it would be desirable to validate the proposed feature extraction method with real measurements from floating wind turbines, the lack of data available from wind energy companies makes this impossible. Thus, the only means of validating any results on floating wind turbines is to use the reference high-fidelity software OpenFast or theoretically, as most of the papers on this topic do. In our case, the main frequencies identified with the proposed methodology are aligned with previous works and are as expected, i.e., the responses of offshore structures are typically dominated by low-frequency components. For example, the fundamental modal frequency of monopile offshore wind turbines is near 0.3 Hz [30] and that of offshore platforms is near 0.8 Hz [31]. In our case, the main frequency identified is 0.605 Hz.

In addition, we have observed the 3P frequency [29]. This is produced by the shadow tower when the rotor is in movement. When the rotor moves at the rated speed, this frequency matches with the TwFADOF1. This indicates that the initial bending frequency of the tower is excited when the rotor moves the blades at its rated speed, causing vibrations.

6. Conclusions and Future Works

The main contribution of this approach is to study the variation in the frequency spectrum of the signal when a DOF of the wind turbine is deactivated. This allows us to relate this variation to the specific DOF that is deactivated. This process is iteratively executed for every DOF in order to identify the main vibration modes. On the other hand, to study the frequency spectrum, we estimate the PSD based on the FFT of the vibration signals. The displacement signals of the wind turbine are obtained with a software simulation tool that enables the deactivation of the various DOFs. This methodology has been successfully validated with the OpenFast software and the NREL 5 MW ITI Barge FOWT.

A series of experiments have been systematically carried out to analyze the relationship between each degree of freedom and the acceleration signal of the tower displacement along the x- and y-axes. The main conclusion that has been derived is that there is a peak at the frequency of 0.0097 Hz that is mainly due to PtfmSgDOF (platform horizontal surge translation) in the x- and y-axes, i.e., the fore–aft and side–side modes, respectively. Considering only the y-axis, this peak is also influenced by the degrees of freedom PtfmSwDOF (platform horizontal sway translation) and FlapDOF1 (first flapwise blade mode).

The 0.085 Hz peak for side-to-side acceleration is mainly due to PtfmSwDOF, although PtfmSgDOF and TwSSDOF1 (first side-to-side tower bending mode) also affect it. PtfmRDOF and PtfmPDOF have a minor impact on this peak. Finally, TwSSDOF1 (first side-to-side tower bending mode) is primarily responsible for the side-to-side accelera-

tion peak at 0.6 Hz. However, the PtfmSgDOF and PtfmRDOF degrees of freedom also have an impact.

It is worth mentioning that the first bending frequency of the tower coincides with the 3P frequency at 0.605 Hz when the wind turbine is operating at the nominal speed. This means that the rotor moving the blades at the rated speed excites the first bending frequency of the tower back and forth, producing vibrations. It is therefore strongly recommended to implement active tower damping strategies to reduce this effect. On the other hand, the modes of the blades, such as the flap and edge in particular, influence the acceleration of the top of the tower along the *y*-axis. Interestingly, the first flapwise blade mode, FlapDOF1, does not show any particular affinity towards regions of fore–aft acceleration peaks.

As the main lines of future work, we can highlight the evaluation of the proposal with different wind turbines, the development of pitch controllers to dampen the vibration modes identified in this study, and the expansion of the methodology to work with different wind and wave profiles.

Author Contributions: M.S.-A.: Conceptualization, Methodology, Software, Validation, Writing—Original Draft Preparation. J.-E.S.-G.: Conceptualization, Methodology, Formal Analysis, Supervision, Software, Writing—Original Draft Preparation, Review and Editing. M.S.: Conceptualization, Validation, Writing—Review and Editing, Supervision, Funding Acquisition. M.T.-R.: Conceptualization, Writing—Review and Editing. All authors have read and agreed to the published version of the manuscript.

Institutional Review Board Statement: Not applicable.

Informed Consent Statement: Not applicable.

Data Availability Statement: Data are available upon reasonable request.

Conflicts of Interest: The authors declare no conflict of interest.

References

1. Gomes, I.L.; Melício, R.; Mendes, V.M.; Pousinho, H.M. Wind power with energy storage arbitrage in day-ahead market by a stochastic MILP approach. *Log. J. IGPL* **2020**, *28*, 570–582. [CrossRef]
2. Javadinasab Hormozabad, S.; Gutierrez Soto, M.; Adeli, H. Integrating structural control, health monitoring, and energy harvesting for smart cities. *Expert Syst.* **2021**, *38*, e12845. [CrossRef]
3. Sierra-García, J.E.; Santos, M. Redes neuronales y aprendizaje por refuerzo en el control de turbinas eólicas. *Rev. Iberoam. Autom. Inform. Ind.* **2021**, *18*, 327–335. [CrossRef]
4. Villoslada, D.; Santos, M.; Tomás-Rodríguez, M. General methodology for the identification of reduced dynamic models of barge-type floating wind turbines. *Energies* **2021**, *14*, 3902. [CrossRef]
5. Jahani, K.; Langlois, R.G.; Afagh, F.F. Structural dynamics of offshore Wind Turbines: A review. *Ocean Eng.* **2022**, *251*, 111136. [CrossRef]
6. Duan, F.; Song, Y.; Gao, S.; Liu, Y.; Chu, W.; Lu, X.; Liu, Z. Study on aerodynamic instability and galloping response of rail overhead contact line based on wind tunnel tests. *IEEE Trans. Veh. Technol.* **2023**, *72*, 7211–7220. [CrossRef]
7. Yu, E.; Xu, G.; Han, Y.; Hu, P.; Townsend, J.F.; Li, Y. Bridge vibration under complex wind field and corresponding measurements: A review. *J. Traffic Transp. Eng. (Engl. Ed.)* **2022**, *9*, 339–362. [CrossRef]
8. Tomás-Rodríguez, M.; Santos, M. Modelling and control of floating offshore wind turbines. *Rev. Iberoam. Autom. Inform. Ind.* **2019**, *16*, 4. [CrossRef]
9. Villoslada, D.; Santos, M.; Tomás-Rodríguez, M. TMD stroke limiting influence on barge-type floating wind turbines. *Ocean Eng.* **2022**, *248*, 110781. [CrossRef]
10. Liu, F.; Gao, S.; Tian, Z.; Liu, D. A new time-frequency analysis method based on single mode function decomposition for offshore wind turbines. *Mar. Struct.* **2020**, *72*, 102782. [CrossRef]
11. Pantano, M.N.; Fernández, M.C.; Rodriguez, L.; Scaglia, G.J.E. *Optimización Dinámica Basada en Fourier: Aplicación al Proceso de Producción de Biodiesel*; Universidad Politécnica de Valencia: Valencia, Spain, 2020.
12. Subbulakshmi, A.; Verma, M.; Keerthana, M.; Sasmal, S.; Harikrishna, P.; Kapuria, S. Recent advances in experimental and numerical methods for dynamic analysis of floating offshore wind turbines—An integrated review. *Renew. Sustain. Energy Rev.* **2022**, *164*, 112525. [CrossRef]

13. Jonkman, J.; Butterfield, S.; Musial, W.; Scott, G. *Definition of a 5-MW Reference Wind Turbine for Offshore System Development (No. NREL/TP-500-38060)*; National Renewable Energy Laboratory (NREL): Golden, CO, USA, 2009.
14. Pezeshki, H.; Adeli, H.; Pavlou, D.; Siriwardane, S.C. State of the art in structural health monitoring of offshore and marine structures. In Proceedings of the Institution of Civil Engineers-Maritime Engineering, Portsmouth, UK, 25–27 January 2023; Thomas Telford Ltd.: London, UK, 2023; Volume 176, pp. 89–108.
15. Johannessen, M. Concept Study and Design of Floating Offshore Wind Turbine Support Structure. Master's Thesis, KTH Royal Institute of Technology, School of Engineering Sciences, Stockholm, Sweden, 2018.
16. Karimirad, M.; Moan, T. A simplified method for coupled analysis of floating offshore wind turbines. *Mar. Struct.* **2012**, *27*, 45–63. [CrossRef]
17. Namik, H.; Stol, K. Individual blade pitch control of a spar-buoy floating wind turbine. *IEEE Trans. Control Syst. Technol.* **2013**, *22*, 214–223. [CrossRef]
18. Ahn, H.; Ha, Y.J.; Kim, K.H. Load Evaluation for Tower Design of Large Floating Offshore Wind Turbine System According to Wave Conditions. *Energies* **2023**, *16*, 1862. [CrossRef]
19. Norén-Cosgriff, K.; Kaynia, A.M. Estimation of natural frequencies and damping using dynamic field data from an offshore wind turbine. *Mar. Struct.* **2021**, *76*, 102915. [CrossRef]
20. Niu, X.; Chen, X.; Qiu, Z.; Wang, H.; Xie, A. Effects of scour on the first natural frequency of monopile in different layered foundations. *Ocean Eng.* **2022**, *265*, 112580. [CrossRef]
21. Zeng, X.; Shi, W.; Feng, X.; Shao, Y.; Li, X. Investigation of higher-harmonic wave loads and low-frequency resonance response of floating offshore wind turbine under extreme wave groups. *Mar. Struct.* **2023**, *89*, 103401. [CrossRef]
22. Deng, Y.; Zhang, S.Y.; Zhang, M.; Gou, P. Frequency-dependent aerodynamic damping and its effects on dynamic responses of floating offshore wind turbines. *Ocean Eng.* **2023**, *278*, 114444. [CrossRef]
23. Gao, S.; Liu, F.; Jiang, C. Improvement study of modal analysis for offshore structures based on reconstructed displacements. *Appl. Ocean Res.* **2021**, *110*, 102596. [CrossRef]
24. Jonkman, J.M.; Buhl, M.L., Jr. *Fast User's Guide-Updated August 2005 (No. NREL/TP-500-38230)*; National Renewable Energy Laboratory (NREL): Golden, CO, USA, 2005.
25. Uicker, J.J., Jr.; Pennock, G.R.; Shigley, J.E. *Theory of Machines and Mechanisms*; Cambridge University Press: Cambridge, UK, 2023.
26. Branlard, E.; Giardina, D.; Brown, C.S. Augmented Kalman filter with a reduced mechanical model to estimate tower loads on a land-based wind turbine: A step towards digital-twin simulations. *Wind Energy Sci.* **2020**, *5*, 1155–1167. [CrossRef]
27. Simulink Mathworks. 2023. Available online: https://es.mathworks.com/products/simulink.html (accessed on 27 June 2023).
28. MATLAB Mathworks. 2023. Available online: https://es.mathworks.com/products/matlab.html (accessed on 27 June 2023).
29. Dolan, D.S.; Lehn, P.W. Simulation model of wind turbine 3p torque oscillations due to wind shear and tower shadow. In Proceedings of the 2006 IEEE PES Power Systems Conference and Exposition, Atlanta, GA, USA, 29 October–1 November 2006; pp. 2050–2057.
30. Dong, X.; Lian, J.; Wang, H.; Yu, T.; Zhao, Y. Structural vibration monitoring and operational modal analysis of offshore wind turbine structure. *Ocean Eng.* **2018**, *150*, 280–297. [CrossRef]
31. Ji, C.Y.; Xue, H.Z.; Shi, X.H.; Gaidai, O. Experimental and numerical study on collapse of aged jacket platforms caused by corrosion or fatigue cracking. *Eng. Struct.* **2016**, *112*, 14–22. [CrossRef]